

# Bicontinuous Soft Solids with a Gradient in Channel Size

David J. French, Andrew B. Schofield, and Job H. J. Thijssen\*

This paper presents examples of bicontinuous interfacially jammed emulsion gels (“bijels”) with a designed gradient in the channel size along the sample. These samples are created by quenching binary fluids which have a gradient in particle concentration along the sample, since the channel size is determined by the local particle concentration. A gradient in local particle concentration is achieved using a two-stage loading process, with different particle volume fractions in each stage. Confocal microscopy and image analysis are used to quantitatively measure the channel size of the bijels. Bijels with a gradient in channel size of up to  $2.8\% \text{ mm}^{-1}$  have been created. Such tailored soft materials could act as templates for energy materials optimized for both high ionic transport rates (high power) and high interfacial area (high energy density), potentially making them useful in novel energy applications.

while Mohraz et al. have developed 3D Ni/Ni(OH)<sub>2</sub> composite electrodes<sup>[16]</sup> and ZnO electrodes.<sup>[17]</sup> Similarly, Zekoll et al. have fabricated hybrid electrolytes composed of bicontinuous microchannels of ceramic lithium-ion electrolyte and a nonconducting polymer,<sup>[18]</sup> while Cai et al. have developed polystyrene-filled bicontinuous structures using ethylene carbonate/xylene bijel templates.<sup>[19]</sup> Recently, Ching et al. demonstrated a method using partially miscible mixtures of solvent and poly(ethylene glycol) to create macroporous bijel-templated materials in timescales of minutes rather than hours.<sup>[20]</sup>

## 1. Introduction

Bicontinuous interfacially jammed emulsion gel (Bijels), which are bicontinuous emulsions stabilized by solid colloidal particles, were first predicted in simulations in 2005,<sup>[1]</sup> and were first realized experimentally in 2007.<sup>[2]</sup> Bijels consist of two interpenetrating fluid channels, with channel sizes typically around 10 μm, and a layer of colloidal particles at the interface between the two fluids. The particle layer is jammed, preventing the liquid channels from coarsening, yielding a kinetically stable structure with a large interfacial area between the two fluids (even though the particles occupy ≈90% of the interface, the remaining interstitial area is still large, on the order of  $1 \text{ m}^2 \text{ mL}^{-1}$  of sample).<sup>[3–5]</sup> Bijels usually have channels which are approximately uniform in size across the sample,<sup>[6]</sup> although Haase et al. have produced narrow bijel fibers with a gradient in channel size due to solvent transfer-induced phase separation.<sup>[7,8]</sup>


The bicontinuous structure and large interfacial-area-to-volume ratio of bijels make them promising candidates for use in novel energy materials, especially since they can be (post)-processed to allow the initial fluid channels to be replaced with other materials.<sup>[9–14]</sup> For example, Lee et al. have used water-lutidine bijels as scaffolds to synthesize porous gold monoliths,<sup>[15]</sup>

Whilst the large interfacial area of bijels makes them a promising candidate for novel energy materials, increasing that interfacial area by reducing the channel size also results in a reduced rate of diffusion through the sample,<sup>[21]</sup> limiting the electrodes' performance.<sup>[22]</sup> To try and optimize both the interfacial area and the diffusive transport rate, we have designed and developed 3D bijels which have a gradient in channel size (see **Figure 1a**)—which should allow material to diffuse quickly into the sample through the large channels at one end, whilst maintaining a large interfacial area at the other (see **Figure 1b**). This structure is similar to that of blood vessels, where a gradient in channel width, from arteries to capillaries, optimizes the rates at which blood is transported around the body and at which substances transfer between blood vessels and surrounding cells.<sup>[23]</sup>

Whilst we draw inspiration from potential applications in advanced energy-storage materials, there are other arenas where bijels with a gradient in channel size may well be useful. For example, thermal management of integrated circuit (IC) components is a major challenge in microelectronics.<sup>[24]</sup> One of the current methods involves thermally conductive porous frameworks with phase-change material in the pores.<sup>[25]</sup> In these composites, heat gets conducted through the backbone and then absorbed as latent heat by the phase-change material. Bicontinuous materials are attractive here, as one channel can act as the thermal conductor, with the other channel containing the phase-change material. Bicontinuous materials with a gradient in pore size may well be particularly appealing, as thermal gradients are larger close to the actual IC components. Another potential application is in membrane filters: a gradient in pore size along the direction of flow can provide enhanced performance in terms of filter lifetime. This is because the gradient in pore size can mitigate effects of fouling: the upstream pores is where fouling begins, so if these pores are larger, then that will help postpone clogging of the filter.<sup>[26]</sup>

In this paper, we create bijels using two fluids (ethylene glycol and nitromethane) which are not miscible at room

D. J. French, A. B. Schofield, J. H. J. Thijssen  
SUPA School of Physics & Astronomy  
The University of Edinburgh  
Peter Guthrie Tait Road, Edinburgh, Scotland EH9 3FD, UK  
E-mail: j.h.j.thijssen@ed.ac.uk

 The ORCID identification number(s) for the author(s) of this article can be found under <https://doi.org/10.1002/admi.202102307>.

© 2022 The Authors. Advanced Materials Interfaces published by Wiley-VCH GmbH. This is an open access article under the terms of the Creative Commons Attribution License, which permits use, distribution and reproduction in any medium, provided the original work is properly cited.

DOI: 10.1002/admi.202102307

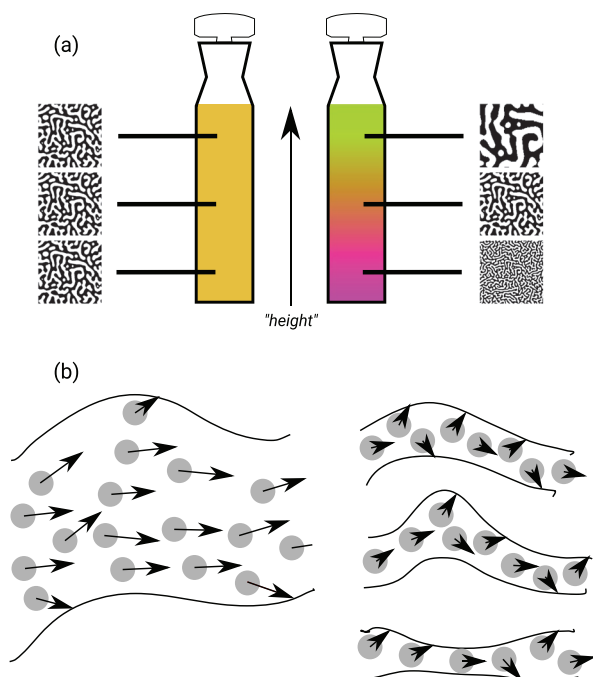


**Figure 1.** a) Schematics of bijel samples without (left) and with (right) gradients in channel size. b) Schematics showing how a gradient in channel size could help optimize transport rate and interfacial area. When the channel size is large (left), diffusion of reactant (gray spheres) along the channel is relatively quick, but the relative interfacial area between channels is low, limiting the reaction rate at the interface. When the channel size is small (right), a greater reaction rate is possible due to more interfacial area being available per unit volume, but the movement of reactants along the channel is reduced.

temperature, but which become miscible above  $\approx 45$  °C<sup>[27]</sup> (see Experimental Section). When the sample is mixed together above this critical temperature and subsequently quenched through the critical point (by immersing the sample in room temperature water), the two liquids separate by spinodal decomposition.<sup>[1]</sup> We ensure separation by spinodal decomposition rather than nucleation by fixing the mass ratio of the two liquids at 64:36 (nitromethane:ethylene glycol), such that the quench goes through the critical point.<sup>[10,28]</sup> The inclusion of neutrally wetting colloidal silica particles in the mixture arrests this separation, as the particles adsorb to the liquid–liquid interface and jam when the liquids’ interfacial area is approximately equal to the total cross-sectional area of the particles. The channel size in a bijel,  $L$ , is therefore proportional to the particle radius,  $r_p$ , and inversely proportional to the particle concentration,  $\phi_p$ .<sup>[3,5]</sup> Since the timescale of fluid–fluid separation is much shorter than that of particle diffusion,<sup>[29]</sup> we can create bijels with a gradient in channel size by having a gradient in particle concentration before the quench

$$L(z) \propto \frac{r_p}{\phi_p(z)} \quad (1)$$

where we create  $\phi_p(z)$  using a two-stage loading process (Figure 2, see Experimental Section). In the remainder of this paper, we use confocal microscopy, absorbance measurements

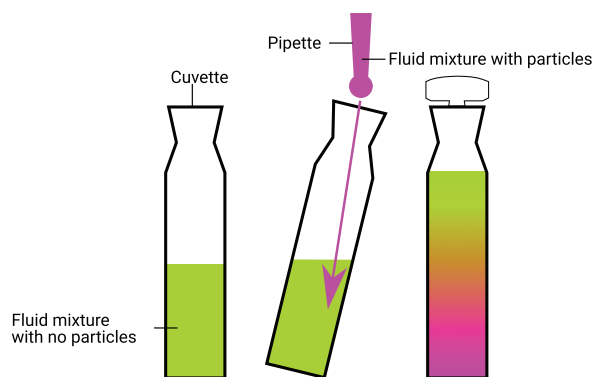


**Figure 2.** Schematic showing preparation of nonuniform bijel. Left: The preheated cuvette is initially partially filled with a mixture of nitromethane and ethylene glycol which contains no particles (green). Centre: a mixture of nitromethane and ethylene glycol which does contain particles (magenta) is gently added to the cuvette using a pipette, so that it runs down the edge of the cuvette. Right: this creates a dispersion with a gradient in particle concentration which, when quenched, yields a bijel with a gradient in channel size.

and image analysis to show that these samples have a statistically significant gradient in channel size.

## 2. Results

Photographs and confocal microscopy images of bijels, with and without gradients in channel size, are shown in Figure 3. Both samples have average particle volume fractions of 2%. The confocal images in Figure 3b clearly show that the channel size increases with height in the sample. The photograph also shows that the sample is darker at the bottom, due to increased scattering of light at smaller channel sizes and concurrently higher particle concentration.

The absorbance,  $A(z)$ , of two bijel samples, one with a uniform channel size and one with a gradient in channel size, is shown in Figure 4b,d. This shows that the measured absorbance is approximately unchanged along the length of the uniform sample but decreases with height in the sample with a gradient in channel size. This is expected, since smaller bijel channels will cause more scattering and hence appear darker in the transmission images. We have also used transmission images to measure the particle volume fraction,  $\phi_p(z)$ , in the samples prior to quenching (Figure 4a,c). The absorbance of a pre-quench sample is related to the local number density,  $n(z)$ , of particles by the Beer–Lambert law

$$T(z) = 10^{-\alpha b n(z)} \quad (2)$$

$$A(z) = -\log_{10} T(z) \propto n(z) \quad (3)$$

where  $\alpha$  is a constant and  $b$  is the path length of the sample.<sup>[30]</sup> Hence, Figure 4e, which shows how the absorbance in each of the samples changes as a function of height in the cuvette, corroborates the relationship between the prequench local particle volume fraction and the postquench channel widths, as expected from Equation (1).

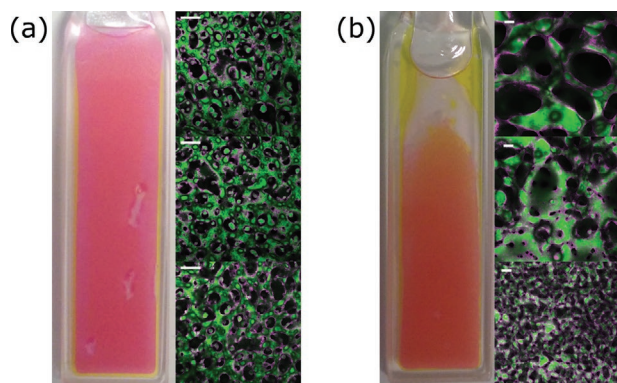


**Figure 3.** a) A bijel sample with no gradient in channel size. b) A bijel sample with a gradient in channel size. In the photographs the cuvettes are 1.25 cm wide; the scale bars in the confocal images are 100  $\mu\text{m}$ . In the confocal images, the green channel is the fluorescein-labeled ethylene glycol, the magenta channel is the rhodamine B-labeled silica and the black is the nitromethane channel.

**Figure 5** shows how the channel width changes with height in bijel samples, both for samples with a designed gradient and for control samples made using a conventional protocol. The normalized lengthscale is calculated by dividing the channel width by the channel width measured at the bottom of the same sample. The 48 data points for the nonuniform data are taken from eight separate bijel samples (1 to 8), and the 17 data points for the uniform data are taken from three separate bijel samples (I to III). Qualitatively, these results suggest that our method to produce non-uniform bijels successfully creates bijels with a gradient in lengthscale.

The coefficient of determination,  $R^2$ , for a linear line of best fit through the nonuniform data is 0.43, corresponding

to a Student's  $t$  value of 5.85. We can therefore reject the null hypothesis that the gradient is zero in the case of the non-uniform data, with  $p < 10^{-6}$ .<sup>[31]</sup> For the uniform data,  $R^2 = 0.008$  and  $t = 0.35$ , and so we cannot reject the null hypothesis that the gradient is zero in this case ( $p > 0.3$ ). Notably,  $R^2$  is a measure of how much better a fit of the functional form  $y = mx + c$  is than a fit of the functional form  $y = \bar{y}$ . If the slope  $m$  is close to 0, then there is little difference between these two fits, which explains why  $R^2$  is small for the uniform data, that is, any variation in the uniform data is due to noise rather than any correlation between the variables. Hence, the statistical analysis confirms that our method is successfully creating bijels with a gradient in lengthscale.

Finally, we note that the gradient in measured lengthscale (Figure 5 (left)) is lower than that predicted by the gradient in local particle concentration (Figure 4, Equation (1)). One might argue that this is due to spinodal decomposition causing some local mixing before jamming occurs. However, the lengthscale of particle movement during spinodal decomposition is expected to be small compared to the channel width, otherwise particles would not get efficiently trapped at the liquid–liquid interface and hence a bijel would not form. Alternative explanations include polydispersity in the particle size distribution and Equation (2) not holding at the particle volume fractions used here; further experiments may provide a definitive explanation.

### 3. Conclusion

We have created and characterized bijels which have a gradient in channel size by developing a simple method which creates particle dispersions with a gradient in particle concentration. Since the channel size of a bijel is determined by the local

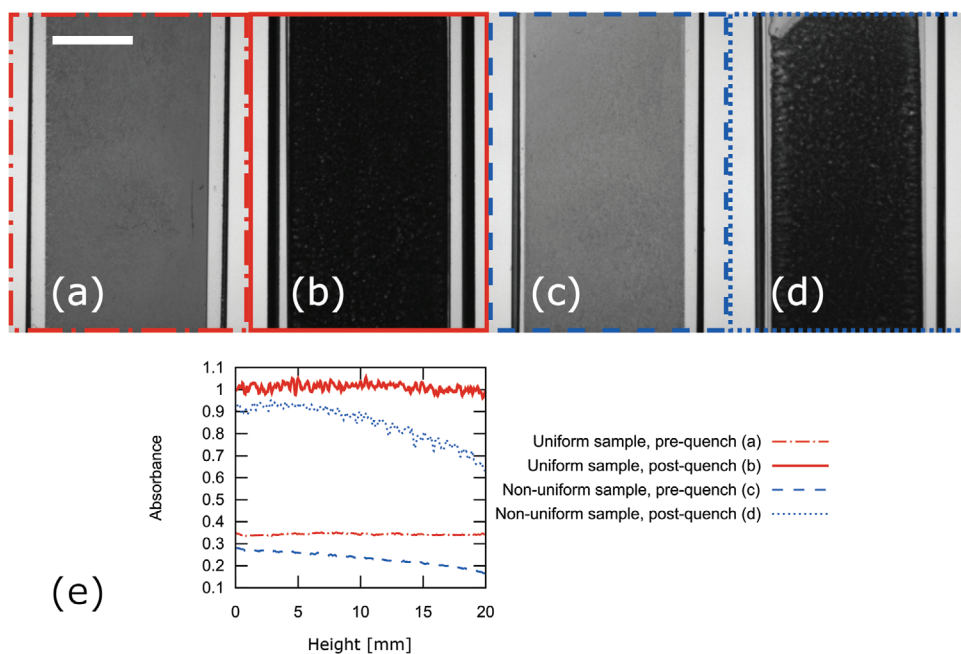


**Figure 4.** Top: photographs of cuvettes containing a,b) uniform and c,d) nonuniform bijel mixtures a,c) pre- and b,d) post-quench. The scale bar is 0.5 cm. Bottom: e) graph showing the measured absorbance in the cuvettes as a function of height.

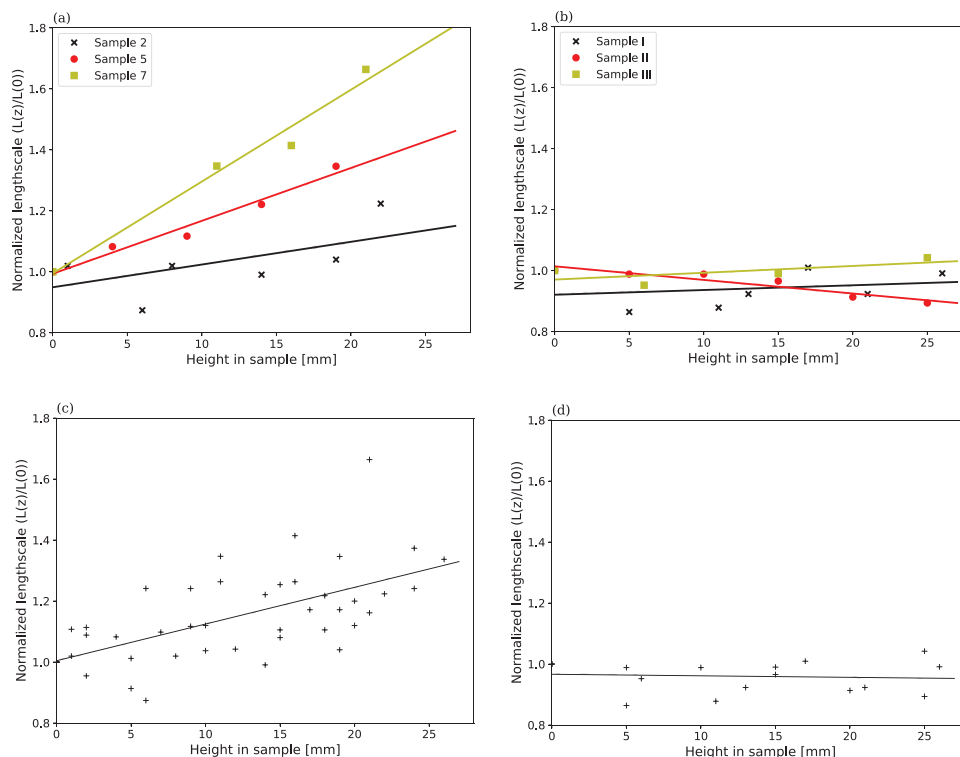


**Figure 5.** Graphs of channel size against height in a) a representative selection of three nonuniform bijels in different symbols and colors, b) all three uniform bijels in different symbols and colors, c) nonuniform bijel samples 1 to 8, and d) uniform bijel samples I to III. The lines are linear least-squares fits for each dataset.

particle concentration, this leads to a gradient in the resultant bijel. We have quantitatively compared these nonuniform bijels to conventional uniform bijels.

We envisage that other methods for creating binary fluids with a gradient in particle concentration will also lead to bijels with a gradient in channel width. Such methods could include the use of polydisperse particle dispersions, which would create a gradient in particle concentration as they sediment, and the agitation of previously-sedimented particle dispersions. Methods for more finely controlling the local particle concentration would also lead to more complex bijel geometries being realized. Finally, external fields may well be promising: Rumble et al. showed that centrifugation can be used to obtain a gradient in channel size, though it also aligns both channels perpendicularly to the direction of the centrifugal force.<sup>[32]</sup>

Tailored soft structures such as those we have described here could be processed in exactly the same way as those in refs. [10,16], in order to create electrodes which have a gradient in pore size; ref. [10] also reports the rheology of (uniform) bijels of nitromethane-ethanediol/silica and its link to processability. Our gradient-bijel method could be particularly useful if methods to create a gradient in particle concentration can be combined with novel techniques which have the potential to scale up the volume of bijels produced, such as direct mixing/homogenization<sup>[33,34]</sup> and phase inversion.<sup>[35]</sup> Our method could also be used in conjunction with the methods described in ref. [20] to create bijel-templated materials with a gradient in channel size, using rapid selective polymerization. Finally, we have suggested that bijels with a gradient in channel size could

find application in advanced energy-storage materials, thermal management in microelectronics and membrane filters.

## 4. Experimental Section

**Materials:** Monodisperse, spherical rhodamine B-labeled fluorescent silica particles were synthesized by following a modified Stöber method.<sup>[36,37]</sup> The silica particles were washed ten times with distilled water, and were then hydrophobized using hexamethyldisilazane (HMDS) (Aldrich, 99.9%) in a solution of ethanol (Fisher, 99.8%) and ammonia (Fisher, 35%).<sup>[27,38–40]</sup> The amount of HMDS used is varied to ensure that the particles are neutrally wetting at the fluid–fluid interface (non-neutrally wetting particles result in an emulsion being formed<sup>[27,41,42]</sup>); the amount of HMDS used ranged from 0.1 to 0.7 g, a typical amount was 0.5 g. Prior to being used to form bijels, the particles were dried in an oven (Binder VD 23) at 170 °C for 30 min at atmospheric pressure before being ground up using a spatula and dried for a further 60 min at 170 °C under full vacuum. The average particle diameter and polydispersity were calculated as 600 nm and 20% by measuring 200 individual particles in a scanning electron microscope image (see Supporting Information). For the purposes of calculating particle volume fractions the particle density was assumed to be 1750 kg m<sup>-3</sup>.<sup>[37]</sup> The size and shape of the particles were checked qualitatively using confocal microscopy.

Nitromethane (Acros Organics, 99+%), ethylene glycol (Sigma-Aldrich, 99.8%) and fluorescein acid (Aldrich) were used as supplied.

**Bijel Fabrication Approach:** The appropriate amount of dried silica particles was placed in a 7 mL glass vial, and the appropriate masses of nitromethane and (fluorescein-labeled) ethylene glycol were added. A typical sample would contain silica (0.03 g), nitromethane (0.64 g), and ethylene glycol (0.36 g). The vial was then placed in an ultrasonic bath (VWR USC300T) for ≈10 min to disperse the particles. Hot water



was used in the bath so that the two fluids also became miscible whilst the particles dispersed. Following dispersal, the vial was placed in an aluminum block which had been preheated to 70 °C. To produce uniform bijels (samples I–III), a preheated glass pipette was then used to transfer the sample into a preheated glass cuvette (Starna type 21 glass cell, 1 mm path length), which was quickly quenched by submersing it in cold water (19 °C; room temperature was 24 °C). To produce nonuniform bijels (samples 1–8), the preheated cuvette was first (approximately) half-filled with a mixture of nitromethane and ethylene glycol (nitromethane:ethylene glycol mass ratio = 64:36;  $\phi_p = 0$ ), before the particle dispersion (nitromethane:ethylene glycol mass ratio = 64:36;  $\phi_p \approx 3\%$ ) was gently added to the cuvette. When the dispersion was added, it ran down the inside edge of the cuvette, mixing with the fluid that was already in the cuvette to form a dispersion with a gradient in particle concentration (high at the bottom of the cuvette, low at the top). A schematic of this process is shown in Figure 2.

**Characterization and Image Analysis:** A Zeiss LSM 700 confocal microscope, coupled to a Zeiss Axio Observer Z1 inverted microscope, was used to perform confocal microscopy. A 10 mW max, 488 nm solid-state laser was used to excite the fluorescein-labeled ethylene glycol and a 10 mW max, 555 nm solid-state laser was used to excite the rhodamine B-labeled silica particles; emission filters were used as appropriate. Imaging was carried out using Zeiss Plan-Neofluar objective lenses: 10× (0.3NA), 20× (0.4NA), and 40× (0.6NA).

A Krüss DSA100 tensiometer was used to take bright field images of cuvettes containing binary fluid mixtures, and of the bijels produced by quenching these mixtures. The plot profile command in ImageJ was used to measure the grayscale values in the samples as a function of height in the cuvettes. These grayscale values were used to calculate the transmission through the sample as a function of height,  $T(z)$ , by normalizing by the grayscale values measured for a cuvette filled with a binary fluid with  $\phi_p = 0$ . Transmission  $T(z)$  was converted to absorbance  $A(z)$  using Equation (3).

Quantitative image analysis was carried out using GNU Octave.<sup>[43]</sup> The green (ethylene glycol) channel from each confocal image was used, and the following protocol employed. First a Gaussian filter was used to smooth the image slightly, then the image was thresholded so that 48% of pixels were white and 52% were black. These fractions were chosen as these were the relative volumes of the ethylene glycol-rich and ethylene glycol-poor phases, respectively.<sup>[27]</sup> The fast Fourier transform (FFT) of the thresholded image was then taken. Following ref. [32], the radially-averaged FFT was fitted to the sum of two Lorentzian functions

$$\gamma = \frac{A}{1 + \left(\frac{x}{w_1}\right)^2} + \frac{B}{1 + \left(\frac{x}{w_2}\right)^2} + C \quad (4)$$

where  $\gamma$  is the intensity,  $x$  is the distance in the FFT in  $\mu\text{m}^{-1}$  and  $A$ ,  $B$ ,  $C$ ,  $w_1$ , and  $w_2$  are fitting parameters. The full width at half maximum (FWHM) was calculated from the fitted equation. The typical lengthscale in the image was taken as the reciprocal of the FWHM, following ref. [32].

Statistical analysis of the measured lengthscales was carried out by fitting data to simple linear regressions and calculating the coefficient of determination,  $R^2$ , using

$$R^2 = \frac{\left(\sum_i (x_i - \bar{x})(y_i - \bar{y})\right)^2}{\sum_i (x_i - \bar{x})^2 \sum_i (y_i - \bar{y})^2} \quad (5)$$

where  $x_i$  and  $y_i$  are the co-ordinates for the  $i$ th datapoint, and  $\bar{x}$  and  $\bar{y}$  are mean values of  $x$  and  $y$ .  $R^2$  is also known as the square of the Pearson product-moment correlation coefficient.

**Data:** The research data presented in this publication are available on the Edinburgh DataShare repository.<sup>[44]</sup>

## Supporting Information

Supporting Information is available from the Wiley Online Library or from the author.

## Acknowledgements

The authors thank the Engineering and Physical Sciences Research Council (EPSRC, UK) for providing funding via Grant EP/P007821/1 and P. S. Clegg for useful initial discussions.

## Conflict of Interest

The authors declare no conflict of interest.

## Data Availability Statement

The data that support the findings of this study are openly available in Edinburgh DataShare at <https://doi.org/10.7488/ds/3185>, reference number 3185.

## Keywords

bicontinuous materials, bijels, confocal, emulsions, energy storage, microscopy, pickering

Received: November 24, 2021

Revised: February 1, 2022

Published online:

- [1] K. Stratford, R. Adhikari, I. Pagonabarraga, J.-C. Desplat, M. E. Cates, *Science* **2005**, *309*, 2198.
- [2] E. M. Herzig, K. A. White, A. B. Schofield, W. C. K. Poon, P. S. Clegg, *Nat. Mater.* **2007**, *6*, 966.
- [3] M. E. Cates, P. S. Clegg, *Soft Matter* **2008**, *4*, 2132.
- [4] A. Mohraz, *Curr. Opin. Colloid Interface Sci.* **2016**, *25*, 89.
- [5] P. M. Welch, M. N. Lee, A. N. G. Parra-Vasquez, C. F. Welch, *Langmuir* **2017**, *33*, 13133.
- [6] P. S. Clegg, J. H. J. Thijssen, in *Bijels: Bicontinuous Particle-stabilized Emulsions* (Ed: P. S. Clegg), Soft Matter Series, The Royal Society of Chemistry, London **2020**, pp. 1–33.
- [7] M. F. Haase, K. J. Stebe, D. Lee, *Adv. Mater.* **2015**, *27*, 7065.
- [8] S. Boakye-Ansah, M. S. Schwenger, M. F. Haase, *Soft Matter* **2019**, *15*, 3379.
- [9] M. N. Lee, A. Mohraz, *Adv. Mater.* **2010**, *22*, 4836.
- [10] M. N. Lee, J. H. J. Thijssen, J. A. Witt, P. S. Clegg, A. Mohraz, *Adv. Funct. Mater.* **2013**, *23*, 417.
- [11] A. Mohraz, T. J. Thorson, in *Bijels: Bicontinuous Particle-stabilized Emulsions* (Ed: P. S. Clegg), The Royal Society of Chemistry, London **2020**, pp. 34–60.
- [12] M. A. Santiago Cordoba, J. S. Spendelow, A. N. G. Parra-Vasquez, L. A. Kuettner, P. M. Welch, C. E. Hamilton, J. A. Oertel, J. G. Duque, E. J. Meierdierks, T. A. Semelsberger, J. C. Gordon, M. N. Lee, *Adv. Funct. Mater.* **2020**, *30*, 1908383.
- [13] A. E. Garcia, C. S. Wang, R. N. Sanderson, K. M. McDevitt, Y. Zhang, L. Valdevit, D. R. Mumm, A. Mohraz, R. Ragan, *Nanoscale Adv.* **2019**, *1*, 3870.
- [14] K. M. McDevitt, T. J. Thorson, E. L. Botvinick, D. R. Mumm, A. Mohraz, *Materialia* **2019**, *7*, 100393.
- [15] M. N. Lee, M. A. Santiago-Cordoba, C. E. Hamilton, N. K. Subbaiyan, J. G. Duque, K. A. D. Obrey, *J. Phys. Chem. Lett.* **2014**, *5*, 809.
- [16] J. A. Witt, D. R. Mumm, A. Mohraz, *J. Mater. Chem. A* **2016**, *4*, 1000.

- [17] K. M. McDevitt, D. R. Mumm, A. Mohraz, *ACS Appl. Energy Mater.* **2019**, *2*, 8107.
- [18] S. Zekoll, C. Marriner-Edwards, A. K. O. Hekselman, J. Kasemchainan, C. Kuss, D. E. J. Armstrong, D. Cai, R. J. Wallace, F. H. Richter, J. H. J. Thijssen, P. G. Bruce, *Energy Environ. Sci.* **2018**, *11*, 185.
- [19] D. Cai, F. H. Richter, J. H. J. Thijssen, P. G. Bruce, P. S. Clegg, *Mater. Horiz.* **2018**, *5*, 499.
- [20] H. Ching, T. J. Thorson, B. Paul, A. Mohraz, *Mater. Adv.* **2021**, *2*, 5067.
- [21] M. M. Mezedur, M. Kaviani, W. Moore, *AIChE J.* **2002**, *48*, 15.
- [22] R. Härmas, R. Palm, M. Härmas, M. Pohl, H. Kurig, I. Tallo, E. Tee, I. Vaas, R. Väli, T. Romann, O. Oll, R. Kanarbik, K. Liivand, J. Eskusson, J. Kruusma, T. Thomberg, A. Jänes, P. Miidla, E. Lust, *Electrochim. Acta* **2018**, *283*, 931.
- [23] L. S. Costanzo, *Physiology*, 6th ed., Philadelphia, PA **2018**.
- [24] S. Tawfick, M. De Volder, D. Copic, S. J. Park, C. R. Oliver, E. S. Polsen, M. J. Roberts, A. J. Hart, *Adv. Mater.* **2012**, *24*, 1628.
- [25] G. Li, X. Zhang, J. Wang, J. Fang, *J. Mater. Chem. A* **2016**, *4*, 17042.
- [26] P. Sanaei, L. J. Cummings, *Phys. Rev. Fluids* **2018**, *3*, 094305.
- [27] J. W. Tavacoli, J. H. J. Thijssen, A. B. Schofield, P. S. Clegg, *Adv. Funct. Mater.* **2011**, *21*, 2020.
- [28] J. A. Witt, D. R. Mumm, A. Mohraz, *Soft Matter* **2013**, *9*, 6773.
- [29] E. Kim, K. Stratford, R. Adhikari, M. E. Cates, *Langmuir* **2008**, *24*, 6549.
- [30] D. F. Swinehart, *J. Chem. Educ.* **1962**, *39*, 333.
- [31] D. Howell, *Statistical Methods for Psychology*, 7th ed., Wadsworth, Cengage Learning, Belmont, CA **2010**.
- [32] K. A. Rumble, J. H. J. Thijssen, A. B. Schofield, P. S. Clegg, *Soft Matter* **2016**, *12*, 4375.
- [33] D. Cai, P. S. Clegg, T. Li, K. A. Rumble, J. W. Tavacoli, *Soft Matter* **2017**, *13*, 4824.
- [34] C. Huang, J. Forth, W. Wang, K. Hong, G. S. Smith, B. A. Helms, T. P. Russell, *Nat. Nanotechnol.* **2017**, *12*, 1060.
- [35] J. Li, H. Sun, M. Wang, *Langmuir* **2020**, *36*, 14644.
- [36] W. Stöber, A. Fink, E. Bohn, *J. Colloid Interface Sci.* **1968**, *26*, 62.
- [37] A. van Blaaderen, A. Vrij, *Langmuir* **1992**, *8*, 2921.
- [38] N. Hijnen, D. Cai, P. S. Clegg, *Soft Matter* **2015**, *11*, 4351.
- [39] M. C. Capel-Sanchez, L. Barrio, J. M. Campos-Martin, J. L. G. Fierro, *J. Colloid Interface Sci.* **2004**, *277*, 146.
- [40] T. I. Suratwala, M. L. Hanna, E. L. Miller, P. K. Whitman, I. M. Thomas, P. R. Ehrmann, R. S. Maxwell, A. K. Burnham, *J. Non-Cryst. Solids* **2003**, *316*, 349.
- [41] K. A. White, A. B. Schofield, P. Wormald, J. W. Tavacoli, B. P. Binks, P. S. Clegg, *J. Colloid Interface Sci.* **2011**, *359*, 126.
- [42] F. Jansen, J. Harting, *Phys. Rev. E* **2011**, *83*, 046707.
- [43] J. W. Eaton, D. Bateman, S. Hauberg, R. Wehbring, *GNU Octave version 5.2.0 manual: a high-level interactive language for numerical computations* **2020**, <https://www.gnu.org/software/octave/doc/v5.2.0/>
- [44] The University of Edinburgh, Edinburgh DataShare, **2021**, <https://doi.org/10.7488/ds/3185>